The Journal of Chemical Physics

Oxygen NMR of high-density and low-density amorphous ice

Cite as: J. Chem. Phys. **156**, 084503 (2022); https://doi.org/10.1063/5.0080333
Submitted: 30 November 2021 • Accepted: 20 January 2022 • Published Online: 22 February 2022

Lars Hoffmann, Joachim Beerwerth, Mischa Adjei-Körner, et al.

COLLECTIONS

Paper published as part of the special topic on Slow Dynamics

This paper was selected as Featured

The Journal of Chemical Physics ARTICLE scitation.org/journal/jcp

Oxygen NMR of high-density and low-density amorphous ice

Cite as: J. Chem. Phys. 156, 084503 (2022); doi: 10.1063/5.0080333
Submitted: 30 November 2021 • Accepted: 20 January 2022 •
Published Online: 22 February 2022

Lars Hoffmann,[1,a)] Joachim Beerwerth,[1] Mischa Adjei-Körner,[1] Violeta Fuentes-Landete,[2] Christina M. Tonauer,[2] Thomas Loerting,[2] and Roland Böhmer[1]

AFFILIATIONS

[1] Fakultät Physik, Technische Universität Dortmund, 44221 Dortmund, Germany
[2] Institute of Physical Chemistry, University of Innsbruck, Innrain 52c, A-6020 Innsbruck, Austria

Note: This paper is part of the JCP Special Topic on Slow Dynamics.
[a)] **Author to whom correspondence should be addressed:** lars.hoffmann@tu-dortmund.de

ABSTRACT

Using oxygen-17 as a nuclear probe, spin relaxometry was applied to study the high-density and low-density states of amorphous ice, covering temperatures below and somewhat above their glass transitions. These findings are put in perspective with results from deuteron nuclear magnetic resonance and with calculations based on dielectrically detected correlation times. This comparison reveals the presence of a wide distribution of correlation times. Furthermore, oxygen-17 central-transition echo spectra were recorded for wide ranges of temperature and pulse spacing. The spectra cannot be described by a single set of quadrupolar parameters, suggesting a distribution of H–O–H opening angles that is broader for high-density than for low-density amorphous ice. Simulations of the pulse separation dependent spin-echo spectra for various scenarios demonstrate that a small-step frequency diffusion process, assigned to the presence of homonuclear oxygen–oxygen interactions, determines the shape evolution of the pulse-separation-dependent spectra.

I. INTRODUCTION

The scientific interest in producing and exploring supercooled water and amorphous ices has a long history.[1,2] Here, it may suffice to refer to a few reviews that convey how stimulating, sometimes "weird," and often controversial the findings regarding liquid and solid waters are.[3–5]

Much of the current activity on the amorphous ices dates back to the discovery that apart from vapor deposited amorphous water,[1] a second, highly dense amorphous form of H_2O can be formed by compression[6] and that using suitably applied pressures, one can switch among high-density amorphous (HDA) and low-density amorphous (LDA) ice states.[7] By now, the existence of two liquid waters seems to be well established.[8,9] Yet, the possible paths through the complex phase diagram of H_2O, including its no-man's land and the nature of the glass transitions, are still under intense debate.[10–13] Various routes leading to the formation of amorphous ices, e.g., via cold deposition of micrometer-sized droplets, were discovered[14] and explored not the least in order to clarify whether water vitrified by rapid (~10^6 K/s) quenching displays the salient features known from the compression-induced amorphous ices.[15]

For the amorphous ices, it took a long while before equilibrated HDA (eHDA, here for simplicity called HDA) could be produced in an annealed, stabilized form[16–18] so that water's second glass transition could be discovered[19] or before it was clear whether or not differently produced noncrystalline low-density states are structurally[20] and dynamically[21] equivalent. Now, it is well-established that annealing at 129 K (or above) for at least 90 min leads to a relaxation of their structures[22] and to the formation of LDA-II (in the following simply called LDA).

One of the major challenges in this field centers on the proper understanding of the nature of HDA's and LDA's glass transitions and of the resulting high-density and low-density (liquid) forms, sometimes called LDL and HDL. To address the corresponding questions, a wide range of experimental and computational methods has been applied to investigate them.[23]

In Fig. 1, we illustrate some of the findings that enabled us to determine time constants from calorimetry[19] and dielectric spectroscopy.[19,24] One recognizes how various time scales can be assessed from the calorimetric onsets ($T_{g,\mathrm{HDA}} \approx 114$ K and $T_{g,\mathrm{LDA}} \approx 136$ K) and from the dielectric loss peaks. From Fig. 1, it also becomes clear that the time scales for HDA widely differ from those

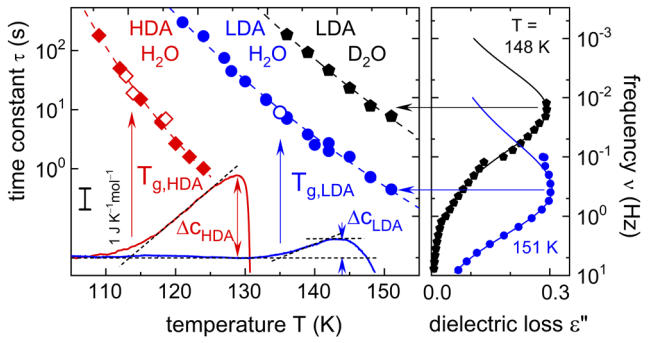

FIG. 1. The frame on the left visualizes how the time scales (open symbols) and the glass transition temperatures $T_{g,HDA}$ and $T_{g,LDA}$ of HDA and LDA, respectively, are determined from the calorimetric data (solid curves[19]) for various scanning rates. The shown data refer to heating rates of 10 K/min. For LDA, the heat capacity step is only $\Delta c_{LDA} \sim 1$ J K^{-1} mol^{-1}, while for HDA, the step size is considerably larger. The horizontal arrows highlight how the dipolar reorientation time scales (closed symbols) were determined from dielectric loss maxima (frame on the right), while "thawing" protonated LDA made from H_2O and from D_2O.[24]

for LDA and that a major H/D isotope effect (here illustrated for LDA) exists.

For the study of the amorphous ices, also techniques such as vibrational spectroscopy[25–28] and nuclear magnetic resonance (NMR)[29–33] were used. The latter experimental method is exploited for the present study as well. For a wide range of glass forming materials, NMR yielded important insights into their dynamics near the glass transition.[34–37]

While proton NMR is most useful to study fast dynamics in water's fluid and moderately supercooled regimes[38–41] as well as in crystalline ice,[42] deuteron NMR, particularly for the crystalline ices, has proven itself as a sensitive technique to unravel important details also in the regime of slower motions.[42–44]

One of the reasons why only few ^{2}H NMR studies of the *amorphous* ices exist is the range of spin lattice relaxation times T_1 from several hundred to thousand seconds near 100 K and below.[29,33] This is almost prohibitively long for an in-depth study of the D_2O dynamics in the noncrystalline states. Notable exceptions are the ^{2}H NMR works of Scheuermann *et al.* and Löw *et al.* who probed the fast dynamics on the time scale of the inverse Larmor frequency (typically corresponding to a few nanoseconds) using spin relaxometry[30,31] and furthermore explored the ultraslow dynamics on and beyond the millisecond regime.[33] However, at the corresponding temperatures, impending crystallization effects were partially affecting the experiments and thus had to be taken into account in the analysis of the results. In the 140–150 K range, LDA crystallizes to a stacking-disordered phase I.[45]

Apart from the ^{1}H and ^{2}H (and the radioactive ^{3}H[46,47]) nuclear probes, ^{17}O is the only other NMR active isotope that was primarily applied to study pure liquid water[39,40,48–50] but can be exploited in studies of neat HDA and LDA as well. Recently, this quadrupolar nucleus is becoming increasingly popular.[51] At least in crystalline ice, ^{17}O spin–lattice relaxation times were found to be much shorter as compared to those measured for ^{2}H.[52] The present work was to some extent motivated by the expectation that this advantage can be exploited also in ^{17}O NMR studies of the noncrystalline forms of water.

II. EXPERIMENTAL DETAILS

Water from Sigma-Aldrich with a 40%–45% isotopic ^{17}O enrichment was used to produce the samples. HDA was prepared and decompressed at 140 K to a pressure of 0.2 GPa as described in Ref. 53. After pressure release, it was transferred from Innsbruck to Dortmund at ambient pressure and liquid nitrogen temperatures. At 77 K, the sample was crushed to a fine powder and cold-loaded into a borosilicate NMR tube that was sealed with a Teflon cap. The cold HDA-filled tube was inserted into a double-resonance probehead from NMR Service Co. that was precooled to 77 K. The probehead, in turn, was transferred to the about 85 K cold cryostat. The experiments were carried out in a magnetic field $B_0 = 9.4$ T corresponding to a Larmor frequency $\omega_L/2\pi = 54.3$ MHz using a Bruker Avance III 400 spectrometer. Typically, the (solid-state) $\pi/2$ pulses were 2.4 μs long. For the measurements of the T_1 times, a saturation sequence with echo refocusing after a variable waiting time t was used. The longitudinal magnetization recovery $M_z(t)$ was detected using the central $+1/2 \leftrightarrow -1/2$ transition of the ^{17}O nuclei and parameterized in terms of the stretched exponential function

$$\frac{M_z(t) - M_0}{M_i - M_0} = \exp\left[-(t/T_1)^{\mu_1}\right], \quad (1)$$

where M_i denotes the initial magnetization and M_0 denotes the equilibrium magnetization. The exponent μ_1 quantifies the deviations from exponential relaxation. A small degree of (intrinsic) nonexponentiality is expected for quadrupolar nuclei, such as ^{17}O.[54–57]

Spin–spin relaxation times T_2 were recorded after application of a $\pi/2$-Δ-π pulse sequence, where Δ designates the pulse separation (also called the echo delay). The decay of the resulting transverse magnetization $M_{xy}(\Delta)$ was fitted using another stretched exponential function

$$M_{xy}(\Delta) = M_0 \exp\left[-(2\Delta/T_2)^{\mu_2}\right], \quad (2)$$

where μ_2 is the corresponding Kohlrausch exponent. For the detection of T_2 and for the acquisition of the "exorcycled"[58] $\pi/2$-Δ-π spectra (from typically 128 to 512 scans), continuous wave 50 W proton decoupling was applied. Unless noted otherwise, a Gaussian apodization with $\sigma = 2\pi \times 500$ Hz was employed. The frequency scale is referenced with respect to liquid $H_2{}^{17}O$. During each measurement, the temperature stability in the variable temperature insert from Oxford Instruments was better than ±0.2 K. The overall heating and cooling rates, including temperature stabilization and data acquisition, typically were about 3–4 K/day.

III. RESULTS

A. ^{17}O spin–lattice relaxation times

Immediately after transferring the cold sample to the cryostat, measurements of T_1 and T_2 and also of the absorption spectra were taken after thermal stabilization was achieved at the desired temperature.

In Fig. 2, we plot the longitudinal magnetization recovery recorded for HDA in a wide temperature range. The data are presented on normalized scales. The good overlap of these recoveries

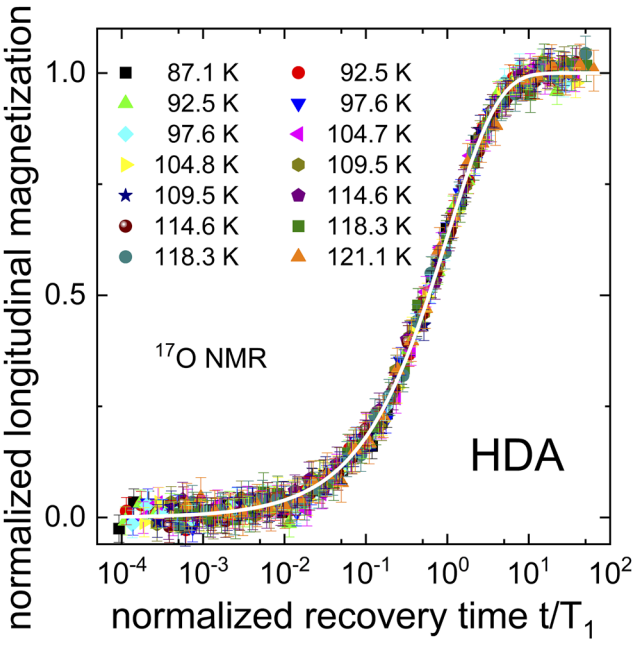

FIG. 2. Amplitude normalized longitudinal magnetization recovery of HDA plotted vs the reduced time t/T_1. The (white) line represents a Kohlrausch fit using Eq. (1) and an exponent $\mu_1 = 0.7$.

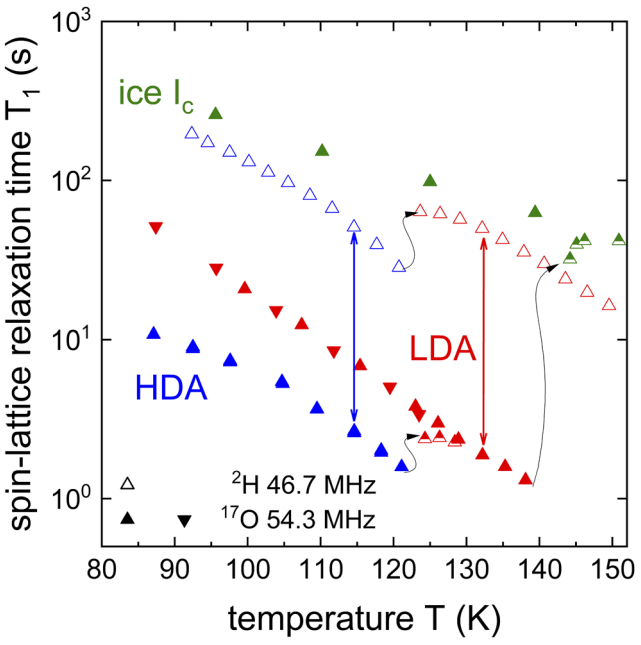

FIG. 3. Temperature dependent spin–lattice relaxation times T_1 as measured using ^{2}H NMR (open triangles) at a Larmor frequency of 46.7 MHz[31] and using ^{17}O NMR (filled triangles) at 54.3 MHz from this work. Triangles pointing up were taken during heating runs, triangles pointing down in cooling runs, and half-filled symbols directly after the transitions had taken place. The colored arrows are meant to indicate that at a given temperature the ^{17}O spin–lattice relaxation times are shorter by a factor of roughly 20 (for HDA) or 25 (for LDA) than their counterparts measured using ^{2}H NMR.

demonstrates that in a wide temperature range, the shape of $M(t)$ is essentially invariant. It is well known that, in general, $M(t)$ is expected to evolve in a nonexponential manner, describable in terms of a sum of three exponentials with relative weights that depend on the exact excitation conditions.[54] For a simple parameterization of $M(t)$, we use Eq. (1) and find an exponent $\mu_1 = 0.7$, which suggests the presence of an underlying distribution of correlation times. The mean spin–lattice relaxation time is $\langle T_1 \rangle = T_1\, \Gamma(1/\mu_1)/\mu_1 \approx 1.27\, T_1$, where Γ denotes the gamma function. The Appendix demonstrates that the exponent $\mu_1 = 0.7$ describes the ^{17}O spin–lattice relaxation also of LDA.

For the two amorphous ices, the resulting ^{17}O spin–lattice relaxation times are summarized in Fig. 3. At the lowest temperatures accessed in this work, T_1 of HDA is about 10 s long. With an increase in temperature, T_1 becomes shorter until near 124.3 K, the transition to the low-density state reveals itself as a step-like increase in T_1. The resulting LDA sample was then successively heated further to ≈129 K, i.e., to a temperature sufficiently below the transition to the stacking-disordered crystalline phase I and (during the measurements) was kept there for about 15 h so that the equilibration to LDA-II could take place.

Further T_1 data were taken while recooling what thus is LDA-II (here for simplicity called LDA) from ≈129 K to about 87 K. Then, the sample was heated until another, much larger jump in T_1 to relatively long values occurred near 141 K. This jump corresponds to the crystallization of our sample and thus to the formation of ice I. Then, the transformed sample was cooled from about 156 to 96 K, and subsequently, further ice I data were recorded upon heating (see Fig. 3).

B. ^{17}O spin–spin relaxation times T_2 and absorption spectra

Transverse magnetization decays were recorded at the same temperature at which T_1 measurements were taken and the resulting $M_{xy}(\Delta)$ curves were parameterized using Eq. (2). During the T_2 experiments, the proton spins were decoupled from the oxygen spins by high-power radio-frequency irradiation and, therefore, do not affect the transverse decay. For HDA and also for LDA, we find that the spin–spin relaxation time $T_2 = 450 \pm 30$ μs and the corresponding exponent $\mu_2 = 0.90 \pm 0.05$ are, within experimental uncertainty, independent of temperature.

An insensitivity to changes in temperature was also observed for the proton-decoupled oxygen-17 absorption spectra: Fig. 4 shows representative examples for HDA, LDA, and (stacking-disordered) ice I. The ^{17}O central-transition spectra reveal the characteristic asymmetric shape expected for H_2O in its condensed phases.

As we will show, the spectra are governed by the second-order quadrupolar interaction. For hexagonal D_2O ice at $T = -10$ to -20 °C,[59] the principal axis values of the electrical field gradient (EFG) tensor of the ^{17}O nucleus are given as $\nu_z = \frac{3}{20} C_Q = \frac{3}{20} eQV_{zz}/h = +0.999$ MHz, $\nu_y = -\frac{3}{20} C_Q \frac{1}{2}(1+\eta) = -0.967$ MHz, and $\nu_x = -\frac{3}{20} C_Q \frac{1}{2}(1-\eta) = -0.032$ MHz.[60,61] Since the EFG tensor is traceless, these quantities are often expressed in terms of only two parameters, i.e., the quadrupolar coupling constant $C_Q = e^2qQ/h = 6.66$ MHz and the asymmetry parameter $\eta_Q = (V_{xx} - V_{yy})/V_{zz}$

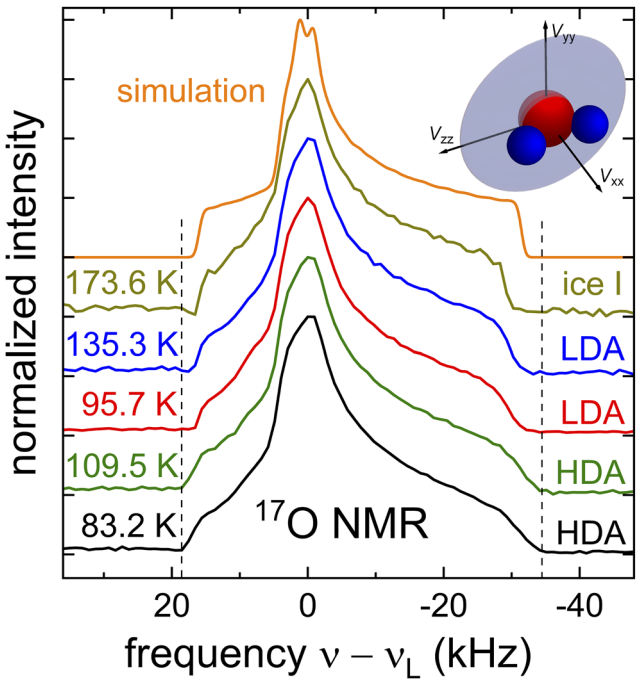

FIG. 4. Absorption spectra of the amorphous ices for different temperatures as recorded for a pulse spacing Δ = 40 μs. The spectra for HDA, LDA, ice I, and the simulated one (uppermost curve) were vertically shifted with respect to each other for visual clarity. The dashed vertical lines highlight that the HDA spectra are somewhat broader than those of LDA and than the spectrum of ice I. For the experimentally determined spectra, an apodization was not applied. The inset on the right hand side depicts a water molecule together with a disk-like structure, which is meant to illustrate the orientation of the EFG tensor characterizing the ^{17}O nucleus along with the principal tensor axes in the molecule-fixed frame.

= 0.935.[60] As sketched in the inset of Fig. 4, the relevant principal axis of the oxygen EFG tensor, which may be thought of as its symmetry axis, is oriented along the C_{2v} axis of the water molecule. This axis coincides with that of the electrical dipole moment vector of the water molecule. Thus, one may expect that oxygen NMR and dielectric spectroscopy provide a similar perspective on the reorientational dynamics within the ices.

For H_2O ice at T = 140 K, a slightly smaller C_Q = 6.43 MHz and η_Q = 0.935 were reported.[62] At least for the crystalline ices, the values of C_Q and η seem to be somewhat sensitive to the structure in which the water molecules are embedded.[63–67]

From Fig. 4, one recognizes that the spectra of HDA are slightly broader and more smeared at the outer edges than those of LDA. However, neither for HDA nor for LDA was an apodization applied. As will be discussed in Sec. IV B, the smearing presumably stems from the variability of the local bonding angles.

As illustrated in the inset of Fig. 4, the x axis of the EFG tensor coincides with the C_{2v} symmetry axis of the water molecule, its y axis is perpendicular to H–O–H plane, and its z axis is parallel to the line that connects the two protons within the water molecule. Since in our powder samples, an isotropic distribution of molecular orientations and thus of tensor orientations is present, it is a simple matter to calculate the expected line shape. The result of this calculation is included in Fig. 4 as well and seen to provide a useful description of the experimental spectra.

In order to be sensitive to the molecular dynamics, temperature dependent line shape changes are often exploited.[34] Line shape changes are expected if the molecular dynamics becomes comparable to or faster than a time scale of about 20 μs, roughly corresponding to the inverse (central-transition) linewidth. The absence of corresponding line shape changes inferred from Fig. 4 implies that on this scale, the molecular dynamics remains slow for HDA and for LDA. In fact, upon heating, the HDA → LDA and the LDA → ice I transitions were observed to take place when the dielectrically detected molecular reorientations times are on the order of 1 s.[19]

Another way to probe molecular dynamics via line shape changes is to record echo spectra as a function of the pulse separation Δ.[68] In Fig. 5, we show central-transition spectra that have been acquired for a wide range of pulse spacings Δ. The Δ dependence of the integrated intensity of these spectra is expected to simply reflect the decay of the transversal magnetization. In order to render possible line shape changes most obvious, the spectra in Fig. 5 are normalized to their intensity at $\nu = \nu_L$. In this representation, one recognizes that the shape in the middle part of the normalized spectra remains largely unchanged, while near the outer edges, variations become obvious.

For a more quantitative analysis of these spectra, prior to normalizing them, we have read out their intensities at the frequency

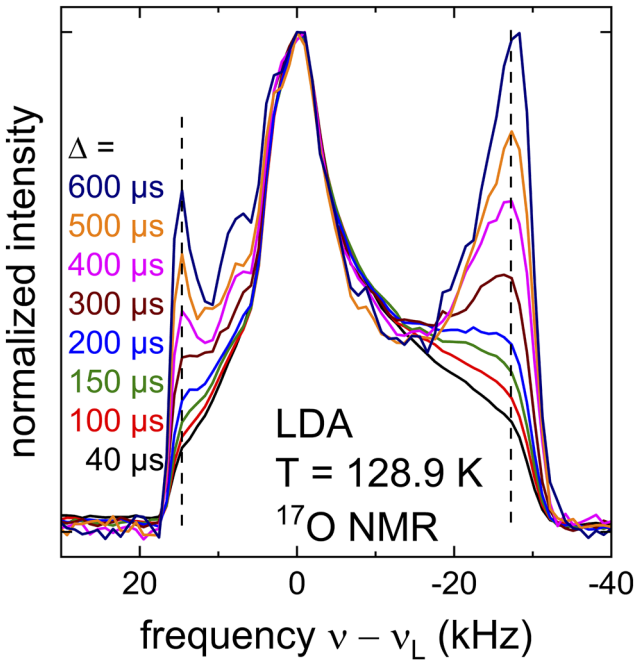

FIG. 5. 90°-Δ–180°-Δ spectra normalized to their intensity at $\nu = \nu_L$. For extended pulse spacings, the overall transversal dephasing time 2Δ is (much) longer than the spin–spin relaxation time T_2. This circumstance leads to a reduced signal-to-noise ratio for the corresponding spectra. The vertical lines mark frequencies of +14.6 and −27.3 kHz.

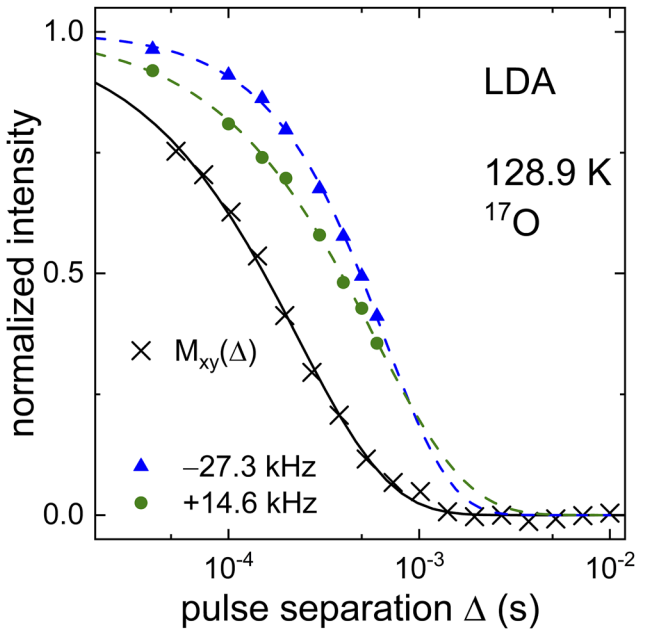

FIG. 6. Decay of the transverse magnetization M_{xy} (crosses) recorded for LDA at 128.9 K and fits using Eq. (2) (solid line) with the initial intensity set to 1. The full symbols refer to the intensity at the specified frequency positions of the pulse-spacing-dependent central-transition spectra read out prior to normalization. The dashed lines guide the eye.

positions marked in Fig. 5. In Fig. 6, we summarize the pulse-spacing-dependent intensities and compare them with the decay of the transversal magnetization that was independently measured at the same temperature. The solid line reflects a fit to these data using Eq. (2) with $T_2 = 450$ s and $\mu_2 = 0.9$, i.e., the parameters already given above. At +14.6 and −27.3 kHz, the transversal decays take roughly two times longer than T_2.

IV. ANALYSIS AND DISCUSSION

A large H/D isotope effect is observed for the amorphous ices,[24,69,70] see also Fig. 1. In comparison with the data from the literature, it is important to point out that for water and ice, an oxygen ($^{16}O/^{18}O$) isotope effect seems to be minute[71–74] and, thus, is not expected to play a significant role for the ^{17}O containing ices that we discuss in the following.

A. Spin relaxation

When trying to determine motional correlation times, spin–lattice relaxation is particularly useful if a T_1 minimum is observed. For the amorphous ices, clearly, this is not the case, see Fig. 3. However, in particular, if motional correlation times are available from other methods, e.g., from dielectric spectroscopy, the spin relaxation times may nevertheless be analyzed. As evident, e.g., from Fig. 1, for HDA and LDA, dielectric time constants are indeed available and their temperature dependence is shown in Fig. 7 in an

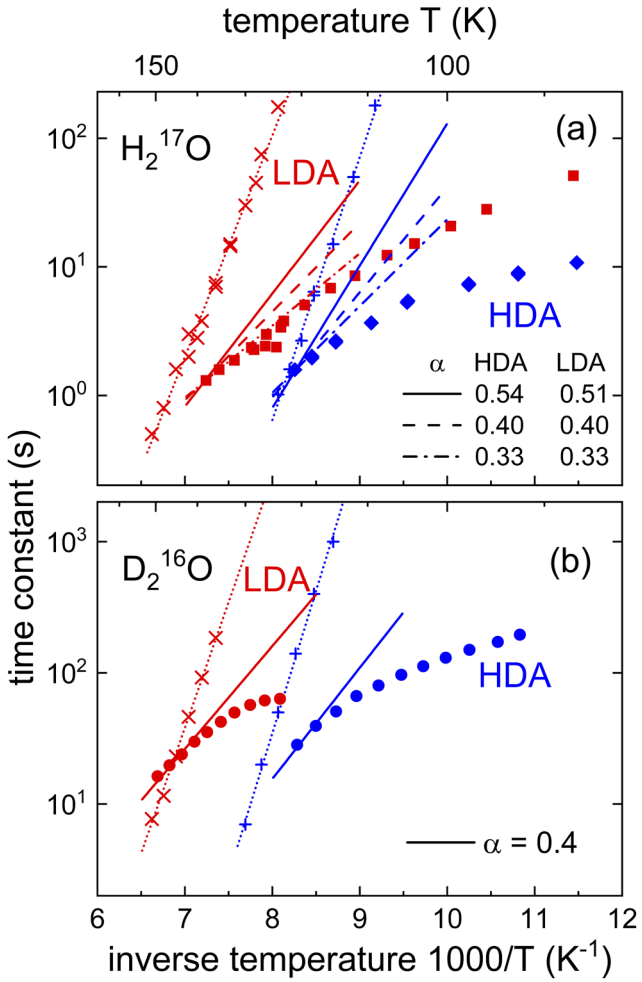

FIG. 7. (a) Arrhenius plot of the spin–lattice relaxation times (full symbols, this work) and the dielectric relaxation times (crosses and dotted lines from Refs. 19 and 75) of protonated LDA and HDA. The label ^{17}O refers only to the NMR results. The solid lines reflect calculations using Eqs. (3), (5), and (7) in conjunction with $\Delta\Omega_Q$ given by the full ^{17}O quadrupolar coupling of 6.66 MHz, the dashed lines with about 2 MHz, and the dashed-dotted lines with about 1 MHz. (b) Same plot for deuterated LDA and HDA but with ^{17}O in natural (0.035%) abundance. The solid lines refer to the full couplings given in the text. Here, the dielectric relaxation times of deuterated LDA and HDA are from Ref. 24 and the ^2H NMR data are from Ref. 31.

Arrhenius representation. In the covered temperature range, the time scales obey an Arrhenius law,

$$\tau = \tau_0 \exp(E/RT), \tag{3}$$

and can be described with an activation energy $E = 39$ kJ/mol[19,75] and a pre-exponential factor $\tau_0 = 3 \times 10^{-17}$ s for protonated HDA as well as with $E = 34$ kJ/mol and $\tau_0 = 1 \times 10^{-12}$ s for protonated LDA, cf. Fig. 7(a). For deuterated HDA, one has $E = 42$ kJ/mol and $\tau_0 = 1 \times 10^{-16}$ s, and for deuterated LDA, one has $E = 37$ kJ/mol and $\tau_0 = 1 \times 10^{-12}$ s,[24,75] cf. Fig. 7(b). Thus, near 125 K, the time scales characterizing the two states differ by a factor of ≈100 for the

deuterated and ≈200 for the protonated samples.[19,24,75] Obviously (see Fig. 3), the ^{2}H and the ^{17}O T_1 times of the two phases differ much less.

To understand this seeming discrepancy, it is useful to analyze the T_1 data quantitatively. We will first consider ^{2}H NMR where spin–lattice relaxation is governed by a quadrupolar relaxation mechanism, i.e., by orientational fluctuations of the EFG tensor with respect to the external magnetic field so that[76]

$$\frac{1}{T_{1,^2\mathrm{H}}^{(\mathrm{Q})}} = \frac{3}{40}\Delta\Omega_{\mathrm{Q},^2\mathrm{H}}^2[J(\omega_\mathrm{L}) + 4J(2\omega_\mathrm{L})]. \tag{4}$$

Here, $J(\omega)$ is the spectral density of these fluctuations. Furthermore, $\Delta\Omega_{\mathrm{Q},^2\mathrm{H}}$ designates the fluctuating part of the quadrupolar coupling $\Omega_\mathrm{Q}/2\pi = C_\mathrm{Q}(1 + \frac{1}{3}\eta^2)^{1/2}$. For HDA, ^{2}H NMR yields e^2qQ/h = 224.6 kHz and η = 0.105, and for LDA, it was found that e^2qQ/h = 217.9 kHz and η = 0.109.[29,31] By contrast to the oxygen EFG tensor (cf. Fig. 4), the main component of the deuteron EFG tensor is oriented along the OD bond and thus couples rather directly not only to flips of the water molecule but also to the dynamics within the OD–O hydrogen bond.

We will now argue that by far, the oxygen nucleus will be dominated by a quadrupolar relaxation mechanism as well. Then, in view of the fact that the ^{17}O quadrupolar coupling is much larger than that for the ^{2}H nuclei, it is no surprise that the ^{2}H-T_1 times are much longer than the ^{17}O-T_1 times. In quantitative terms, for the latter, one has

$$\frac{1}{T_{1,^{17}\mathrm{O}}^{(\mathrm{Q})}} = \frac{3}{625}\Delta\Omega_{\mathrm{Q},^{17}\mathrm{O}}^2[J(\omega_\mathrm{L}) + 4J(2\omega_\mathrm{L})]. \tag{5}$$

Apart from the different (spin dependent) prefactor, for ^{17}O, the fluctuating part of the quadrupolar coupling is expected to be on the order of several megahertz. Other interactions include the heteronuclear O–H dipole coupling, the chemical shift anisotropy, and the homonuclear O–O dipole interaction. Using the gyromagnetic ratio γ_O of oxygen-17 (with spin quantum number I = 5/2), the strength of the latter can be assessed by calculating the corresponding second moment on the basis of the Van Vleck formula,[77]

$$M_2 = \frac{3I(I+1)}{15}\left(\frac{\mu_0}{4\pi}\right)^2\gamma_\mathrm{O}^4\hbar^2\sum_{ij}\frac{1}{r_{ij}^6}. \tag{6}$$

Here, the sum is over all O–O distances r_{ij}. For hexagonal ice, the nearest neighbor distance is $r_{\mathrm{O-O}} \approx 2.76$ Å. Via $\sigma_{\mathrm{OO}} = \sqrt{4w_\mathrm{O}M_2}$, where $w_\mathrm{O} \approx 0.42$ reflects the ^{17}O enrichment, this leads to $\sigma_{\mathrm{OO}}/(2\pi)$ = 312 Hz. This standard deviation relates to a full width at half maximum (FWHM) $\Delta\nu_{1/2}^{\mathrm{OO}} = 2\sqrt{2\ln 2}\,\sigma_{\mathrm{OO}}/2\pi$ = 734 Hz of the corresponding Gaussian distribution. With $r_{\mathrm{O-O}} \approx 2.77$ Å in LDA and $r_{\mathrm{O-O}} \approx 2.82$ Å in HDA from Raman scattering[78] as well as $r_{\mathrm{O-O}} \approx 2.75$ Å in LDA and $r_{\mathrm{O-O}} \approx 2.78$ Å in HDA from x-ray experiments,[79] for the amorphous ices, σ_{OO} will be on the same order of magnitude. Thus, even for the considerable ^{17}O enrichment of our samples, the homonuclear O–O dipole contribution to T_1 relative to that due to the quadrupolar one [cf. Eq. (5)] can be expected to be negligible. The same is true for the contributions arising from the chemical shift anisotropy, which are ≈2 kHz at our field (from the calculated 37 ppm[80]), as well as for the heteronuclear ^{1}H–^{17}O coupling, which was estimated to be about 5 kHz.[81]

In order to describe the experimental T_1 data, also the spectral density has to be known. The classical form due to Bloembergen, Purcell, and Pound (BPP)[82] corresponds to a single exponential relaxation, while the relaxation in the amorphous ices is known to deviate from this behavior. For instance, the high-frequency slope of HDA's dielectric loss is governed by a power law $\varepsilon'' \propto \nu^{-\alpha}$ with an exponent $\alpha \approx 0.5$.[21] This power-law behavior is compatible with that expected from a Cole–Davidson function,[83] which is associated with a spectral density[84]

$$J_{\mathrm{CD}}(\omega) = \frac{\sin[\alpha\,\arctan(\omega\tau)]}{\omega(1+\omega^2\tau^2)^{\alpha/2}}. \tag{7}$$

Here, the parameter $0 < \alpha \le 1$ is a measure for the width of the distribution of correlation times τ, with $\alpha = 1$ corresponding to the BPP case.

In a first step, we analyzed the ^{2}H data shown in Fig. 7(b). Tentatively assuming α = 0.4 and that $\Delta\Omega_{\mathrm{Q},^2\mathrm{H}}$ is given by the full coupling $\Omega_{\mathrm{Q},^2\mathrm{H}}$, we calculated T_1 on the basis of Eqs. (3), (4), and (7). From Fig. 7(b), one recognizes that the computed T_1 indeed matches the experimental spin–lattice relaxation times, however, only at the temperatures just below those at which the amorphous ices undergo a transition. This agreement is not as bad as it may seem because from various NMR studies, it is well known that in the glass transition region, T_1 "bends over" to a behavior characterized by an effective barrier of low energy.[35]

Encouraged by these findings, we now turn to the ^{17}O labeled samples. From Fig. 7(a), we see that for α = 0.4, again, just below the transitions, the measured T_1 times are recovered. However, the predicted temperature dependences of T_1 seem too steep, see the dashed lines. In fact, in the low-temperature regime, i.e., for $\omega_L\tau \gg 1$ which the experimental T_1 data refer to, Eqs. (3), (5), and (7) predict that $T_1 \propto \exp[E_{\mathrm{eff}}/(k_BT)]$ with $E_{\mathrm{eff}} = \alpha E$. The dashed-dotted lines in Fig. 7(a) (again allowing for some deviations at low temperatures) correspond to $E_{\mathrm{eff,HDA}}$ = 13 kJ/mol and $E_{\mathrm{eff,LDA}}$ = 11 kJ/mol. Together with the barriers given above for the T_1 data, this suggests that the exponents are as given in Fig. 7(a). However, the determination of these exponents and the associated fluctuation amplitudes $\Delta\Omega_Q$ is not unambiguous: By imposing the constraint that (only) the T_1 data just below the transitions are captured, for 1 MHz ≤ $\Delta\Omega_{\mathrm{Q},^{17}\mathrm{O}}/2\pi \le 6.66$ MHz, we find that $\alpha_{\mathrm{LDA}} = a_L + b_L \log_{10}[\Delta\Omega_{\mathrm{Q},^{17}\mathrm{O}}/(2\pi$ MHz)] with a_L = 0.30, b_L = 0.24, and $\alpha_{\mathrm{HDA}} = a_H + b_H \log_{10}[\Delta\Omega_{\mathrm{Q},^{17}\mathrm{O}}/(2\pi$ MHz)] with a_H = 0.32 and b_H = 0.25. Although these relations involve fluctuation amplitudes that are much smaller than the full coupling $\Omega_{\mathrm{Q},^{17}\mathrm{O}}$, they still exceed considerably the couplings relating to the other spin interactions discussed above.

Another argument for a possibly reduced fluctuation amplitude of the oxygen coupling comes from comparing Eqs. (4) and (5). Starting from the full couplings, a combination of these equations suggests

$$\frac{T_{1,^2\mathrm{H}}^{(\mathrm{Q})}}{T_{1,^{17}\mathrm{O}}^{(\mathrm{Q})}} = \frac{8}{125}\frac{\Omega_{\mathrm{Q},^{17}\mathrm{O}}^2}{\Omega_{\mathrm{Q},^2\mathrm{H}}^2} \approx 80, \tag{8}$$

which furthermore tacitly assumes that the (shapes of the) spectral densities, the Larmor frequencies (all near 50 MHz), and also the underlying motional processes are basically the same. The latter is only approximately true because during a tetrahedral jump of a water molecule, its O–D bond will reorient by about 109°, while

the C_{2v} axis of the water molecule (and likewise, the oxygen EFG tensor) will reorient by 90°. The experimentally determined ratio of T_1 times of 20–25 (cf. Fig. 2) is, however, roughly four times smaller than suggested by Eq. (8). Assuming that $\Delta\Omega_{Q,^2H} = \Omega_{Q,^2H}$, it, thus, would appear that the fluctuating part of the oxygen coupling is only about $\sqrt{25/80}$, i.e., roughly 50% of the full $\Omega_{Q,^{17}O}$, a reduction that currently we are unable to rationalize. The effective coupling will be further discussed in Sec. IV B.

Finally, we briefly discuss the spin–spin relaxation time: The temperature insensitivity of T_2 suggests that the transversal dephasing is dominated by homonuclear dipolar O–O interactions. Indeed, the "Lorentzian" FWHM $\Delta\nu_{1/2}$ relating to T_2 is $\Delta\nu_{1/2} = 1/(\pi T_2)$ ≈ 700 Hz, which approximately equals the homonuclear "Gaussian" width $\Delta\nu_{1/2}^{OO}$ estimated above (for hexagonal ice).

B. NMR spectra and slow motions

The overall width of the NMR spectrum for ice I, shown in Fig. 4, nicely agrees with that of the simulation. However, despite complete proton decoupling, as compared to the crystalline ice, the amorphous ices display a significant spectral broadening. Its occurrence suggests that the electronic environment at the oxygen site is affected by a distribution of local bonding geometries. The broadening is more pronounced for HDA than it is for LDA.

From neutron scattering work, it has been concluded that in highly dense ices, in particular, in HDA, there is a "considerable degree of hydrogen bond bending in these materials compared to LDA"[20] and also that the most probable of the widely distributed H–O–H opening angles differs from the tetrahedral one. Furthermore, from unpublished neutron work, the width of this bond angle distribution appears to be significantly larger for HDA than for LDA.[85]

Based on a modified Townes–Dailey model, it is known that the EFG parameters depend on the relative directions and occupancies for the lone-pair and OH-bonding orbitals,[66,67,86] with the electronic effects opposing the changes in local geometry.[87] These complexities call for dedicated quantum chemical calculations of the EFG parameters not only for crystalline[88] but also for the amorphous ices. In any case, in view of the neutron diffraction results, it becomes clear that with respect to ice I, the ^{17}O spectra of the amorphous ices are expected to be washed out[89] and that this effect will be stronger for HDA than for LDA in harmony with the experimental observation made from Fig. 4. Furthermore, above, e.g., in relation to Eq. (8), we discussed the spin–lattice relaxation in terms of well-defined EFG parameters. Given a distribution of local charge environments to which the oxygen nucleus is subjected, this tacit assumption may not be fully justified. It remains to be clarified, however, whether and to which extent a distribution of EFG parameters will give rise to reduced effective quadrupolar couplings.

A discussion of the pulse-spacing-dependent spectra shown in Fig. 5 calls for further analysis. From these spectra that are normalized to their peak amplitudes, we observe a relative intensity increase in the frequency ranges from 10 to 15 kHz and from −25 to −30 kHz. The orientation of the oxygen EFG tensor with respect to the external magnetic field—described by the polar angle θ and azimuthal angle ϕ in the usual way[90]—is encoded in the second-order precession frequencies $\omega(\theta,\varphi)$.[91,92] From the color coding of the unit-sphere representation of these frequencies (see Fig. 8), one recognizes that the "red" edge of the spectra corresponds to the angular range centered at $\theta = 90°$ and $\phi = 0°$ and the "blue" edge to $\theta \approx 45°$ and $\phi = 90°$ (and symmetry equivalent combinations of these angles). These ("red" and "blue") angular ranges thus seem unrelated with those expected for, e.g., tetrahedral molecular jumps. One possibility to rationalize this behavior further is in terms of anisotropic spin–spin relaxation times.

To clarify the situation, we simulated the Δ-dependent spectra by assuming various scenarios of how the precession frequencies could be modulated during the total dephasing time 2Δ. Among these scenarios are the isotropic random-jump and rotational-diffusion models[93] as well as an approach that has been used to simulate quasi-tetrahedral motions in hexagonal ice.[62,94] Since the local reorientational geometry of the water molecules in LDA and in hexagonal ice may be anticipated to bear a large

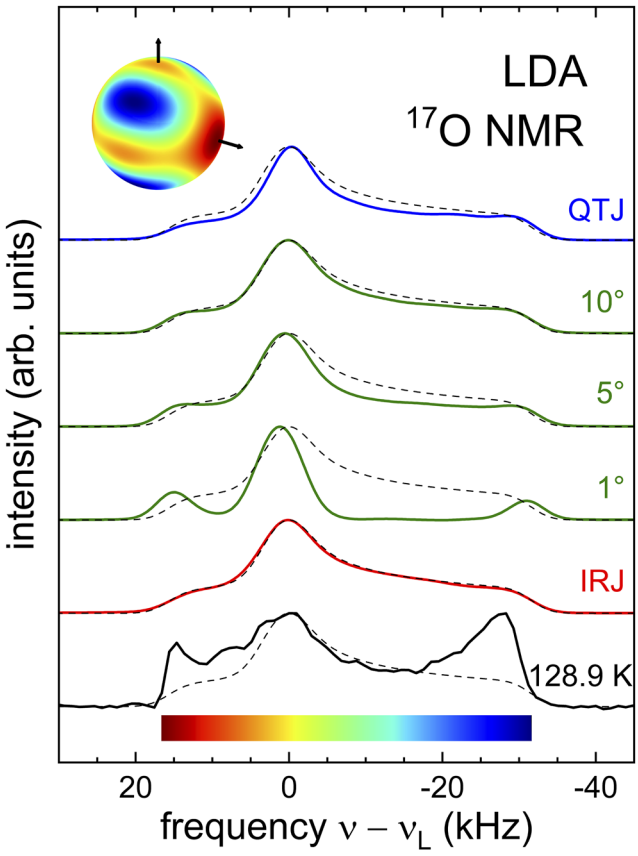

FIG. 8. The experimental spectrum for the longest pulse separation Δ = 600 μs measured at 128.9 K is reproduced from Fig. 5 and compared with the spectra simulated for various scenarios, including (i) the quasi-tetrahedral jump (QTJ) model given in Ref. 62, (ii) the small-step rotational diffusion model with the listed jump angles, and (iii) the isotropic random-jump (IRJ) model. All the simulations refer to Δ = 600 μs, are represented as solid lines, are subjected to an apodization with $\sigma/2\pi$ = 2 kHz, and are normalized to the peak maximum. For reference purposes, the thin dashed lines reproduce the simulated ("rigid-lattice") spectrum from Fig. 4. The colored sphere (for η = 0.935) shows which combinations of angles that enter the precession frequency $\omega(\theta, \varphi)$ contribute to a given spectral position. The arrow pointing to the top corresponds to $\theta = 0$ and the arrow to the side to $\phi = 0$.

degree of similarity, the general trends of the simulated spectra are nevertheless presumed to be relevant for our discussion.

For this work, we use the trajectory-based Monte Carlo (random-walk) algorithm that previously was mostly employed with respect to ^{2}H NMR of glass forming materials.[35,95,96] Analogous simulations were recently exploited also in the framework of the NMR of oxygen[97,98] and other strongly quadrupolarly perturbed nuclei,[99,100] mostly focusing on crystalline materials. Here, we adopt this approach for application to noncrystalline samples.

To mimic a diffusive evolution of the precession frequencies, one may resort either to small-step jumps directly in the frequency domain[101] or approximate them in terms of a succession of reorientational jumps of the EFG tensor about small angles $\Delta\varphi$. Here, $\Delta\varphi \to 0$ corresponds to the limit of rotational diffusion. The simulation of molecular jumps about either a finite fixed or else a random reorientational angle is straightforward if the asymmetry parameter characterizing the relevant tensor vanishes. However, in the presence of a significant asymmetry, $\eta > 0$, of the relevant tensor, additional efforts are required.

For these simulations, viewed from the principal axis system of the EFG tensor, we performed a rotation of this tensor by an angle $\Delta\varphi$ about a randomly chosen reorientation axis (defined by two randomly chosen Euler angles).[102] For each angular jump appearing in the course of a given trajectory of time dependent precession frequencies $\omega(\theta, \phi)$, a new random reorientation axis is determined. To carry out a powder average, when initializing a given trajectory, a randomly oriented external magnetic field was chosen, which was kept fixed for the remainder of that trajectory. To obtain spectra with an acceptable signal-to-noise ratio, typically, 10^5 to 10^6 trajectories were averaged. The orientational life times were drawn from an exponential distribution that was adjusted such that the experimentally observed T_2 (of about 500 μs) resulted.

Figure 8 displays the spectra thus obtained for various scenarios and compares them with the experimentally determined one, all relating to a pulse spacing Δ = 600 μs. To appreciate the effect of this large Δ, the spectra are compared with the simulation for the static spectrum (which is independent of a specific scenario). The model of isotropic rotational random jumps leads to a homogeneous decrease in the spectral intensity with increasing Δ, and thus, after amplitude rescaling, the spectrum is identical to that for $\Delta = 0$. Although the agreement is qualitative at best, small-step rotational diffusion appears to be the only scenario that leads to a relative intensity enhancement near the outer edges of the spectrum. Thus, also the Δ-dependence of the spectra seems to be governed by a small-step frequency change, most likely arising as a consequence of homonuclear oxygen–oxygen interactions.

With the goal to obtain insight also into the *ultraslow* molecular dynamics of crystalline and amorphous ices, deuteron stimulated echoes were previously exploited.[33,44] Oxygen stimulated echoes and two-dimensional exchange NMR were so far applied in studies of hexagonal ice and clathrate hydrates.[92,94,103] However, for these techniques to be useful, the motional correlation times need to be significantly shorter than T_1. A glance at Fig. 7(a) shows that for the amorphous ices, this condition is not fulfilled and that near the transition temperatures, T_1 should be at least about 10 times (for HDA) or at least about 40 times (for LDA) longer than the experimentally observed values $T_{1,\mathrm{exp}}$. In principle, in the slow-motion regime, longer ^{17}O spin–lattice relaxation times can be achieved by resorting to larger Larmor frequencies ω_L. From Eqs. (5) and (7), it follows that $T_1(\omega_L) \propto {\omega_L}^{1+\alpha}$. This relation leads to $T_{1,\mathrm{needed}}/T_{1,\mathrm{exp}} = (B/B_0)^{1+\alpha}$ so that with a Cole–Davidson exponent $\alpha = 0.4$ assumed, for a 10- or 40-fold increase in T_1, very large static magnetic fields B on the order of 50 or 130 T, respectively, would be required. At such field strengths, reduced second-order quadrupolar broadenings and increased chemical-shift-anisotropy related spectral broadenings are expected, with the latter presumably providing only a minor additional spin relaxation channel.

V. CONCLUSIONS

In this work, we measured the longitudinal magnetization recovery and the transversal dephasing of the ^{17}O magnetization for LDA and HDA over a wide temperature range. Well-defined changes in the spin–lattice relaxation times are observed at the HDA → LDA and the LDA → ice I transitions. As compared to the ^{2}H T_1 times, those measured for ^{17}O are 20–25 times shorter. The sets of relaxation times for the two nuclei are analyzed in conjunction with the dielectric relaxation times that are available for the protonated and deuterated amorphous ices. Compatibility of the NMR time scales with those expected on the basis of dielectric spectroscopy is achieved for temperatures just below those at which LDA and HDA undergo a transition to a new amorphous state or the crystalline phase I, respectively. The description of the data requires a distribution of correlation times, here parameterized in terms of a Cole–Davidson parameter of 0.45 ± 0.05. Furthermore, the present analysis raises the possibility that unlike for the deuterons, for the ^{17}O spin–lattice relaxation, the fluctuating part of the quadrupolar coupling is below its full value. With respect to the spin–spin relaxation, it was shown that the dipolar oxygen–oxygen interactions prevail.

As compared to crystalline ice I, the absorption spectra of the amorphous ices display an intrinsic broadening that is more pronounced for HDA than it is for LDA. These broadenings were rationalized in terms of correspondingly large distributions of H–O–H opening angles, a finding that is in harmony with unpublished results from neutron diffraction.[85]

While the shapes of the HDA and LDA spin-echo spectra are largely independent of temperature, a pronounced dependence on the pulse separation Δ was discovered. After scaling to the peak intensity, for large Δ, this phenomenon is easily recognized as a significant relative enhancement near the outer edges of the ^{17}O central-transition spectra. Random-walk simulations were performed for various rotationally induced frequency changes with the goal to test several scenarios. These include quasi-tetrahedral, random reorientational, and small-step jumps. The latter situation was found to give best qualitative agreement with the experimental observations, suggesting that here the oxygen–oxygen magnetic dipole interactions play an important role as well. Finally, it was pointed out that an access to the ultraslow dynamics in the amorphous ices using ^{17}O NMR would require very high magnetic fields.

ACKNOWLEDGMENTS

We thank B. Geil, C. Gainaru, K. Amann-Winkel, and G. Diezemann for stimulating discussions on various aspects related

to this work that was generously supported by the Deutsche Forschungsgemeinschaft under Project No. 413265854. C.M.T. is a recipient of a DOC fellowship of the Austrian Academy of Sciences ÖAW and is supported by the Early Stage Funding 2021 of the University of Innsbruck. We dedicate this work to the late Austen Angell who, not the least in the exploration of supercooled water and amorphous ice, has been a sparkling source of inspiration, advancing the field with countless insightful ideas and seminal experimental and computational contributions.

AUTHOR DECLARATIONS

Conflict of Interest

The authors have no conflicts to disclose.

DATA AVAILABILITY

The data that support the findings of this study are available from the corresponding author upon reasonable request.

APPENDIX: MAGNETIZATION RECOVERY OF LDA

For LDA, the shape of the longitudinal magnetization recovery curves is very similar to that for HDA. Figure 9 displays the data for LDA in a doubly scaled format. This representation highlights that the nonexponentiality of the recoveries is essentially invariant when changing the temperature over a wide range.

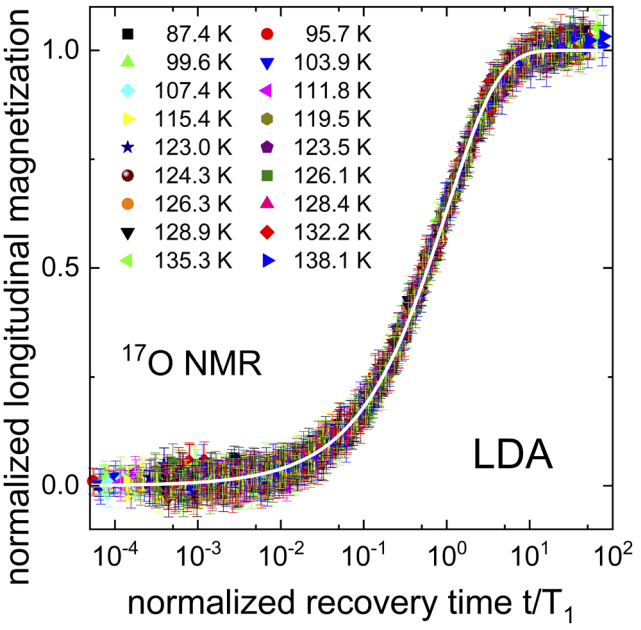

FIG. 9. Analogous to Fig. 2, this plot shows the normalized longitudinal magnetization recovery of LDA vs the reduced time t/T_1. The (white) line represents a Kohlrausch fit using Eq. (1), again with an exponent $\mu_1 = 0.7$.

REFERENCES

[1] E. F. Burton and W. F. Oliver, "X-ray diffraction patterns of ice," Nature **135**, 505 (1935).
[2] C. A. Angell and E. J. Sare, "Vitreous water: Identification and characterization," Science **168**, 280 (1970).
[3] C. A. Angell, "Amorphous water," Annu. Rev. Phys. Chem. **55**, 559 (2004).
[4] C. A. Angell, "Insights into phases of liquid water from study of its unusual glass-forming properties," Science **319**, 582 (2008).
[5] P. Gallo, K. Amann-Winkel, C. A. Angell, M. A. Anisimov, F. Caupin, C. Chakravarty, E. Lascaris, T. Loerting, A. Z. Panagiotopoulos, J. Russo, J. A. Sellberg, H. E. Stanley, H. Tanaka, C. Vega, L. Xu, and L. G. M. Pettersson, "Water: A tale of two liquids," Chem. Rev. **116**, 7463 (2016).
[6] O. Mishima, L. D. Calvert, and E. Whalley, "An apparently first-order transition between two amorphous phases of ice induced by pressure," Nature **314**, 76 (1985).
[7] O. Mishima, "Reversible first-order transition between two H_2O amorphs at ~0.2 GPa and ~135 K," J. Chem. Phys. **100**, 5910 (1994).
[8] H. Tanaka, "Liquid-liquid transition and polyamorphism," J. Chem. Phys. **153**, 130901 (2020).
[9] K. H. Kim *et al.*, "Experimental observation of the liquid-liquid transition in bulk supercooled water under pressure," Science **370**, 978 (2020).
[10] P. H. Handle, T. Loerting, and F. Sciortino, "Supercooled and glassy water: Metastable liquid(s), amorphous solid(s), and a no-man's land," Proc. Natl. Acad. Sci. U. S. A. **114**, 13336 (2017).
[11] C. G. Salzmann, "Advances in the experimental exploration of water's phase diagram," J. Chem. Phys. **150**, 060901 (2019).
[12] L. Kringle, W. A. Thornley, B. D. Kay, and G. A. Kimmel, "Reversible structural transformations in supercooled liquid water from 135 to 245 K," Science **369**, 1490 (2020).
[13] P. Gallo, J. Bachler, L. E. Bove, R. Böhmer, G. Camisasca, L. E. Coronas, H. R. Corti, I. de Almeida Ribeiro, M. de Koning, G. Franzese, V. Fuentes-Landete, C. Gainaru, T. Loerting, J. M. M. de Oca, P. H. Poole, M. Rovere, F. Sciortino, C. M. Tonauer, and G. A. Appignanesi, "Advances in the study of supercooled water," Eur. Phys. J. E **44**, 143 (2021).
[14] E. Mayer, "New method for vitrifying water and other liquids by rapid cooling of their aerosols," J. Phys. Chem. **58**, 663 (1985).
[15] J. Bachler, J. Giebelmann, and T. Loerting, "Experimental evidence for glass polymorphism in vitrified water droplets," Proc. Natl. Acad. Sci. U. S. A. **118**, e2108194118 (2021).
[16] R. J. Nelmes, J. S. Loveday, T. Strässle, C. L. Bull, M. Guthrie, G. Hamel, and S. Klotz, "Annealed high-density amorphous ice under pressure," Nat. Phys. **2**, 414 (2006).
[17] K. Winkel, M. S. Elsaesser, E. Mayer, and T. Loerting, "Water polyamorphism: Reversibility and (dis)continuity," J. Chem. Phys. **128**, 044510 (2008).
[18] J. N. Stern, M. Seidl-Nigsch, and T. Loerting, "Evidence for high-density liquid water between 0.1 and 0.3 GPa near 150 K," Proc. Natl. Acad. Sci. U. S. A. **116**, 9191 (2019).
[19] K. Amann-Winkel, C. Gainaru, H. Nelson, P. H. Handle, M. Seidl, R. Böhmer, and T. Loerting, "Water's second glass transition," Proc. Natl. Acad. Sci. U. S. A. **110**, 17720 (2013).
[20] D. T. Bowron, J. L. Finney, A. Hallbrucker, I. Kohl, T. Loerting, E. Mayer, and A. K. Soper, "The local and intermediate range structures of the five amorphous ices at 80 K and ambient pressure: A Faber-Ziman and Bhatia-Thornton analysis," J. Chem. Phys. **125**, 194502 (2006).
[21] L. J. Plaga, A. Raidt, V. Fuentes Landete, K. Amann-Winkel, B. Massani, T. M. Gasser, C. Gainaru, T. Loerting, and R. Böhmer, "Amorphous and crystalline ices studied by dielectric spectroscopy," J. Chem. Phys. **150**, 244501 (2019).
[22] V. Fuentes-Landete *et al.*, "Crystalline and amorphous ices," in *Water: Fundamentals as the Basis for Understanding the Environment and Promoting Technology*, edited by P. G. Debenedetti, M. A. Ricci, and F. Bruni (IOS, Amsterdam, 2015), Vol. 187, Proceedings of the International School of Physics "Enrico Fermi."
[23] K. Amann-Winkel, R. Böhmer, C. Gainaru, F. Fujara, B. Geil, and T. Loerting, "Colloquium: Water's controversial glass transitions," Rev. Mod. Phys. **88**, 011002 (2016).

[24]C. Gainaru, A. L. Agapov, V. Fuentes-Landete, K. Amann-Winkel, H. Nelson, K. W. Köster, A. I. Kolesnikov, V. N. Novikov, R. Richert, R. Böhmer, T. Loerting, and A. P. Sokolov, "Anomalously large isotope effect in the glass transition of water," Proc. Natl. Acad. Sci. U. S. A. **111**, 17402 (2014).
[25]A. I. Kolesnikov, V. V. Sinitsyn, E. G. Ponyatovsky, I. Natkaniec, and L. S. Smirnov, "Similarity of vibrational spectra of high-density amorphous ice and high-pressure phase ice VI," Physica B **213-214**, 474 (1995).
[26]H. Schober, A. Tölle, M. Koza, F. Fujara, C. A. Angell, and R. Böhmer, "Amorphous polymorphism in ice investigated by inelastic neutron scattering," Physica B **241-243**, 897 (1998).
[27]M. M. Koza, B. Geil, M. Scheuermann, H. Schober, G. Monaco, and H. Requardt, "Vibrational dynamics of very high density amorphous ice studied by high-resolution x-ray spectroscopy," Phys. Rev. B **78**, 224301 (2008).
[28]A. Shalit, F. Perakis, and P. Hamm, "Disorder-suppressed vibrational relaxation in vapor-deposited high-density amorphous ice," J. Chem. Phys. **140**, 151102 (2014).
[29]J. A. Ripmeester, C. I. Ratcliffe, and D. D. Klug, "A ^{1}H and ^{2}H nuclear magnetic resonance study of amorphous ices at 77 K," J. Chem. Phys. **96**, 8503 (1992).
[30]M. Scheuermann, B. Geil, K. Winkel, and F. Fujara, "Deuteron spin lattice relaxation in amorphous ices," J. Chem. Phys. **124**, 224503 (2006).
[31]F. Löw, K. Amann-Winkel, B. Geil, T. Loerting, C. Wittich, and F. Fujara, "Limits of metastability in amorphous ices: ^{2}H-NMR relaxation," Phys. Chem. Chem. Phys. **15**, 576 (2013).
[32]E. Lisitsin-Baranovsky, S. Delage, O. Sucre, O. Ofer, P. Ayotte, and G. Alexandrowicz, "*In situ* NMR measurements of vapor deposited ice," J. Phys. Chem. C **120**, 25445 (2016).
[33]F. Löw, K. Amann-Winkel, T. Loerting, F. Fujara, and B. Geil, "Ultra-slow dynamics in low density amorphous ice revealed by deuteron NMR: Indications of a glass transition," Phys. Chem. Chem. Phys. **15**, 9308 (2013).
[34]K. Schmidt-Rohr and H. W. Spiess, *Multidimensional Solid-State NMR and Polymers* (Academic Press, London, 1994).
[35]K. MacKenzie and M. Smith, *Multinuclear Solid-State Nuclear Magnetic Resonance of Inorganic Materials* (Pergamon, Amsterdam, 2002).
[36]R. Böhmer, G. Diezemann, G. Hinze, and E. Rössler, "Dynamics of supercooled liquids and glassy solids," Prog. Nucl. Magn. Reson. Spectrosc. **39**, 191 (2001).
[37]H. Eckert, "Structural characterization of noncrystalline solids and glasses using solid-state NMR," Prog. Nucl. Magn. Reson. Spectrosc. **24**, 159 (1992).
[38]C. A. Angell, J. Shuppert, and J. C. Tucker, "Anomalous properties of supercooled water: Heat capacity, expansivity, and PMR chemical shift from 0–38%," J. Phys. Chem. **77**, 3092 (1973).
[39]D. Lankhorst, J. Schriever, and J. C. Leyte, "Determination of the rotational correlation time of water by proton NMR relaxation in $H_2{}^{17}O$ and some related results," Ber. Bunsenges. Phys. Chem. **86**, 215 (1982).
[40]J. R. C. van der Maarel, D. Lankhorst, J. de Bleijser, and J. C. Leyte, "On the single-molecule dynamics of water from proton, deuterium and oxygen-17 nuclear magnetic relaxation," Chem. Phys. Lett. **122**, 541 (1985).
[41]J. Qvist, C. Mattea, E. P. Sunde, and B. Halle, "Rotational dynamics in supercooled water from nuclear spin relaxation and molecular simulations," J. Chem. Phys. **136**, 204505 (2012).
[42]R. J. Wittebort, M. G. Usha, D. J. Ruben, D. E. Wemmer, and A. Pines, "Observation of molecular reorientation in ice by proton and deuterium magnetic resonance," J. Am. Chem. Soc. **110**, 5668 (1988).
[43]F. Fujara, S. Wefing, and W. F. Kuhs, "Direct observation of tetrahedral hydrogen jumps in ice Ih," J. Chem. Phys. **88**, 6801 (1988).
[44]B. Geil, T. M. Kirschgen, and F. Fujara, "Mechanism of proton transport in hexagonal ice," Phys. Rev. B **72**, 014304 (2005).
[45]W. F. Kuhs, C. Sippel, A. Falenty, and T. C. Hansen, "Extent and relevance of stacking disorder in 'ice I_c,'" Proc. Natl. Acad. Sci. U. S. A. **109**, 21259 (2012).
[46]R. O. Ramseier, "Self-diffusion of tritium in natural and synthetic ice monocrystals," J. Appl. Phys. **38**, 2553 (1967).
[47]K. Goto, T. Hondoh, and A. Higashi, "Determination of diffusion coefficients of self-interstitials in ice with a new method of observing climb of dislocations by X-ray topography," Jpn. J. Appl. Phys., Part 1 **25**, 351 (1986), and references cited therein. As far as we know, ^{3}H NMR has not been used in ice research.
[48]R. Ludwig, F. Weinhold, and T. C. Farrar, "Experimental and theoretical determination of the temperature dependence of deuteron and oxygen quadrupole coupling constants of liquid water," J. Chem. Phys. **103**, 6941 (1995), and references cited therein.
[49]R. Ludwig, "NMR relaxation studies in water-alcohol mixtures: The water-rich region," Chem. Phys. **195**, 329 (1995).
[50]E. V. Silletta, M. E. Tuckerman, and A. Jerschow, "Unusual proton transfer kinetics in water at the temperature of maximum density," Phys. Rev. Lett. **121**, 076001 (2018).
[51]G. Wu, "^{17}O NMR studies of organic and biological molecules in aqueous solution and in the solid state," Prog. Nucl. Magn. Reson. Spectrosc. **114-115**, 135–191 (2019), and references cited therein.
[52]M. Adjei-Acheamfour and R. Böhmer, "Second-order quadrupole interaction based detection of ultra-slow motions: Tensor operator framework for central-transition spectroscopy and the dynamics in hexagonal ice as an experimental example," J. Magn. Reson. **249**, 141 (2014).
[53]K. Winkel, E. Mayer, and T. Loerting, "Equilibrated high-density amorphous ice and its first-order transition to the low-density form," J. Phys. Chem. B **115**, 14141 (2011).
[54]E. R. Andrew and D. P. Tunstall, "Spin-lattice relaxation in imperfect cubic crystals and in non-cubic crystals," Proc. Phys. Soc., London **78**, 1 (1961).
[55]T. E. Bull, S. Forsén, and D. L. Turner, "Nuclear magnetic relaxation of spin 5/2 and spin 7/2 nuclei including the effects of chemical exchange," J. Chem. Phys. **70**, 3106 (1979).
[56]C.-W. Chung and S. Wimperis, "Measurement of spin-5/2 relaxation in biological and macromolecular systems using multiple-quantum NMR techniques," Mol. Phys. **76**, 47 (1992).
[57]J. Zhu and G. Wu, "Quadrupole central transition ^{17}O NMR spectroscopy of biological macromolecules in aqueous solution," J. Am. Chem. Soc. **133**, 920 (2011).
[58]I. Furó and B. Halle, "2D quadrupolar-echo spectroscopy with coherence selection and optimized pulse angle," J. Magn. Reson. **98**, 388 (1992).
[59]P. Waldstein and S. W. Rabideau, "^{17}O nuclear magnetic resonance of single crystals of D_2O ice," J. Chem. Phys. **47**, 5338 (1967).
[60]H. W. Spiess, B. B. Garrett, R. K. Sheline, and S. W. Rabideau, "Oxygen-17 quadrupole coupling parameters for water in its various phases," J. Chem. Phys. **51**, 1201 (1969).
[61]For the positive sign of C_Q see, e.g., S. G. P. Brosnan and D. T. Edmonds, "Proton fine structure in the nuclear quadrupole double resonance spectrum of ^{17}O naturally abundant in ice at 77 K," J. Mol. Struct. **58**, 23 (1980).
[62]Y. Ba, J. A. Ripmeester, and C. I. Ratcliffe, "Water molecular reorientation in ice and tetrahydrofuran clathrate hydrate from line shape analysis of ^{17}O spin-echo NMR spectra," Can. J. Chem. **89**, 1055 (2010).
[63]D. T. Edmonds, S. D. Goren, A. L. Mackay, A. A. L. White, and W. F. Sherman, "The nuclear quadrupole resonance of ^{2}D and ^{17}O in Ice II," J. Magn. Reson. **23**, 505 (1976).
[64]D. T. Edmonds, S. D. Goren, A. A. L. White, and W. F. Sherman, "Nuclear quadrupole resonance of ^{2}D and ^{17}O in ices V, VI, VIII, and IX," J. Magn. Reson. **27**, 35 (1977).
[65]K. Yamada, K. Deguchi, T. Shimizu, and J. Watanabe, "Line-shape analyses of solid-state ^{17}O NMR spectra for hexagonal ice," Z. Naturforsch., B **69**, 786 (2014).
[66]I. J. F. Poplett, "^{1}H/^{2}H and ^{1}H/^{17}O nuclear quadrupole double-resonance study of several hydroxide compounds. II. The water molecule," J. Magn. Reson. **50**, 397 (1982).
[67]U. Sternberg, "The bond angle dependence of the asymmetry parameter of the oxygen-17 electric field gradient tensor," Solid State Nucl. Magn. Reson. **2**, 181 (1993).
[68]M. Vogel and E. Rössler, "On the nature of slow β-process in simple glass formers: A ^{2}H NMR study," J. Phys. Chem. B **104**, 4285 (2000).
[69]A. L. Agapov, A. I. Kolesnikov, V. N. Novikov, R. Richert, and A. P. Sokolov, "Quantum effects in the dynamics of deeply supercooled water," Phys. Rev. E **91**, 022312 (2015).
[70]V. Fuentes Landete, L. J. Plaga, M. Keppler, R. Böhmer, and T. Loerting, "Nature of water's second glass transition elucidated by doping and isotope substitution experiments," Phys. Rev. X **9**, 011015 (2019).

[71] Y. Nagano, Y. Miyazaki, T. Matsuo, and H. Suga, "Heat capacities and enthalpy of fusion of heavy oxygen water," J. Phys. Chem. **97**, 6897 (1993).
[72] J. J. Shephard and C. G. Salzmann, "Molecular reorientation dynamics govern the glass transitions of the amorphous ices," J. Phys. Chem. Lett. **7**, 2281 (2016).
[73] B. Kutus, A. Shalit, P. Hamm, and J. Hunger, "Dielectric response of light, heavy and heavy-oxygen water: Isotope effects on the hydrogen-bonding network's collective relaxation dynamics," Phys. Chem. Chem. Phys. **23**, 5467 (2021).
[74] S. Ahlmann *et al.*, "Heavy-oxygen and H/D isotope effects in amorphous ices and aqueous acid solutions" (unpublished).
[75] S. Lemke, P. H. Handle, L. J. Plaga, M. Seidl, V. Fuentes-Landete, K. Amann-Winkel, K. W. Köster, C. Gainaru, T. Loerting, and R. Böhmer, "Relaxation dynamics and transformation kinetics of deeply supercooled water: Temperature, pressure, doping, and proton/deuteron isotope effects," J. Chem. Phys. **147**, 034506 (2017).
[76] H. W. Spiess, "Rotation of molecules and nuclear spin relaxation," in *Dynamic NMR Spectroscopy* (Springer, Berlin, 1978), see Chap. 4.1.1, Table 4.4.
[77] A. Abragam, *The Principles of Nuclear Magnetism* (Oxford University Press, Oxford, 1961).
[78] T. Loerting, C. Salzmann, I. Kohl, E. Mayer, and A. Hallbrucker, "A second distinct structural 'state' of high-density amorphous ice at 77 K and 1 bar," Phys. Chem. Chem. Phys. **3**, 5355 (2001).
[79] D. Mariedahl, F. Perakis, A. Späh, H. Pathak, K. H. Kim, G. Camisasca, D. Schlesinger, C. Benmore, L. G. M. Pettersson, A. Nilsson, and K. Amann-Winkel, "X-ray scattering and O–O pair-distribution functions of amorphous ices," J. Phys. Chem. B **122**, 7616 (2018).
[80] T. S. Pennanen, J. Vaara, P. Lantto, A. J. Sillanpää, K. Laasonen, and J. Jokisaari, "Nuclear magnetic shielding and quadrupole coupling tensors in liquid water: A combined molecular dynamics simulation and quantum chemical study," J. Am. Chem. Soc. **126**, 11093 (2004).
[81] W. R. Groves and C. H. Pennington, "Comparison of ^{17}O spin-lattice relaxation solid state NMR studies of pure and doped ices," Chem. Phys. **315**, 1 (2005).
[82] N. Bloembergen, E. M. Purcell, and R. V. Pound, "Relaxation effects in nuclear magnetic resonance absorption," Phys. Rev. **73**, 679 (1948).
[83] D. W. Davidson and R. H. Cole, "Dielectric relaxation in glycerol, propylene glycol, and *n*-propanol," J. Chem. Phys. **19**, 1484 (1951).
[84] P. A. Beckmann, "Spectral densities and nuclear spin relaxation in solids," Phys. Rep. **171**, 85 (1988).
[85] D. T. Bowron, private communication (November 2021).
[86] S. Vega, "On the asymmetry parameter and the principal directions of the electric field gradient tensor in NQR spectroscopy," J. Chem. Phys. **60**, 3884 (1974).
[87] P. L. Cummins, G. B. Bacskay, N. S. Hush, B. Halle, and S. Engström, "The effect of intermolecular interactions on the ^{2}H and ^{17}O quadrupole coupling constants in ice and liquid water," J. Chem. Phys. **82**, 2002 (1985).
[88] M. Alfredsson and K. Hermansson, "Hartree–Fock and DFT calculations of quadrupole coupling constants in water clusters and ice," Chem. Phys. **242**, 161 (1999).
[89] For ^{2}H spectra this seems only exceptionally to be the case, see, e.g., M. Frey, H. Didzoleit, C. Gainaru, and R. Böhmer, "Dynamics in glass forming sulfuric and nitric acid hydrates," J. Phys. Chem. B **117**, 12164 (2013).
[90] P. P. Man, "Quadrupole couplings in nuclear magnetic resonance: General," in *Encyclopedia of Analytical Chemistry*, edited by R. A. Meyers (John Wiley & Sons, Chichester, 2000), p. 12224.
[91] T. Takahashi, "Quadrupole nuclei in inorganic materials," in *Experimental Approaches of NMR Spectroscopy: Methodology and Application to Life Science and Materials Science* (Springer, Singapore, 2018).
[92] M. Adjei-Acheamfour, M. Storek, J. Beerwerth, and R. Böhmer, "Two-dimensional second-order quadrupolar exchange powder spectra for nuclei with half-integer spins. Calculations and an experimental example using oxygen NMR," Solid State Nucl. Magn. Reson. **71**, 96 (2015).
[93] B. Geil, F. Fujara, and H. Sillescu, "^{2}H NMR time domain analysis of ultraslow reorientations in supercooled liquids," J. Magn. Reson. **130**, 18 (1998).
[94] M. Adjei-Acheamfour, J. F. Tilly, J. Beerwerth, and R. Böhmer, "Water dynamics on ice and hydrate lattices studied by second-order central-line stimulated-echo oxygen-17 nuclear magnetic resonance," J. Chem. Phys. **143**, 214201 (2015).
[95] G. Hinze, "Geometry and time scale of the rotational dynamics in supercooled toluene," Phys. Rev. E **57**, 2010 (1998).
[96] M. Vogel and E. Rössler, "Effects of various types of molecular dynamics on 1D and 2D ^{2}H NMR studied by random walk simulations," J. Magn. Reson. **147**, 43 (2000).
[97] J. Beerwerth, M. Storek, D. Greim, J. Lueg, R. Siegel, B. Cetinkaya, W. Hiller, H. Zimmermann, J. Senker, and R. Böhmer, "Two-site jumps in dimethyl sulfone studied by one- and two-dimensional ^{17}O-NMR spectroscopy," J. Magn. Reson., Ser. B **288**, 84 (2018).
[98] J. Beerwerth, R. Siegel, L. Hoffmann, L. S. Plaga, M. Storek, B. Bojer, J. Senker, W. Hiller, and R. Böhmer, "From ultraslow to extremely fast dynamics in sodium nitrate. An ^{17}O NMR study," Appl. Magn. Reson. **51**, 597 (2020).
[99] J. Beerwerth, S. P. Bierwirth, J. Adam, C. Gainaru, and R. Böhmer, "Local and global dynamics of the viscous ion conductors $2Ca(NO_3)_2$-$3KNO_3$ and $2Ca(NO_3)_2$-$3RbNO_3$ probed by ^{87}Rb nuclear magnetic resonance and shear rheology," J. Chem. Phys. **150**, 194503 (2019).
[100] L. Hoffmann, J. Beerwerth, D. Greim, J. Senker, C. Sternemann, W. Hiller, and R. Böhmer, "Reorientational dynamics of trimethoxyboroxine: A molecular glass former studied by dielectric spectroscopy and ^{11}B nuclear magnetic resonance," J. Chem. Phys. **152**, 034503 (2020).
[101] B. Geil, G. Diezemann, and R. Böhmer, "Calculations of stimulated echoes and two-dimensional nuclear magnetic resonance spectra for solids with simple line shapes," J. Chem. Phys. **128**, 114506 (2008).
[102] U. Tracht, A. Heuer, and H. W. Spiess, "Geometry of reorientational dynamics in supercooled poly(vinyl acetate) studied by ^{13}C two-dimensional nuclear magnetic resonance echo experiments," J. Chem. Phys. **111**, 3720 (1999), used a slightly different approach which we understand to involve, in each reorientation step, only a single randomly chosen angle and not, like in our approach, two randomly chosen ones.
[103] M. Adjei-Acheamfour, M. Storek, and R. Böhmer, "Communication: Heterogeneous water dynamics on a clathrate hydrate lattice detected by multi-dimensional oxygen nuclear magnetic resonance," J. Chem. Phys. **146**, 181101 (2017).